Supplementary Figure S1

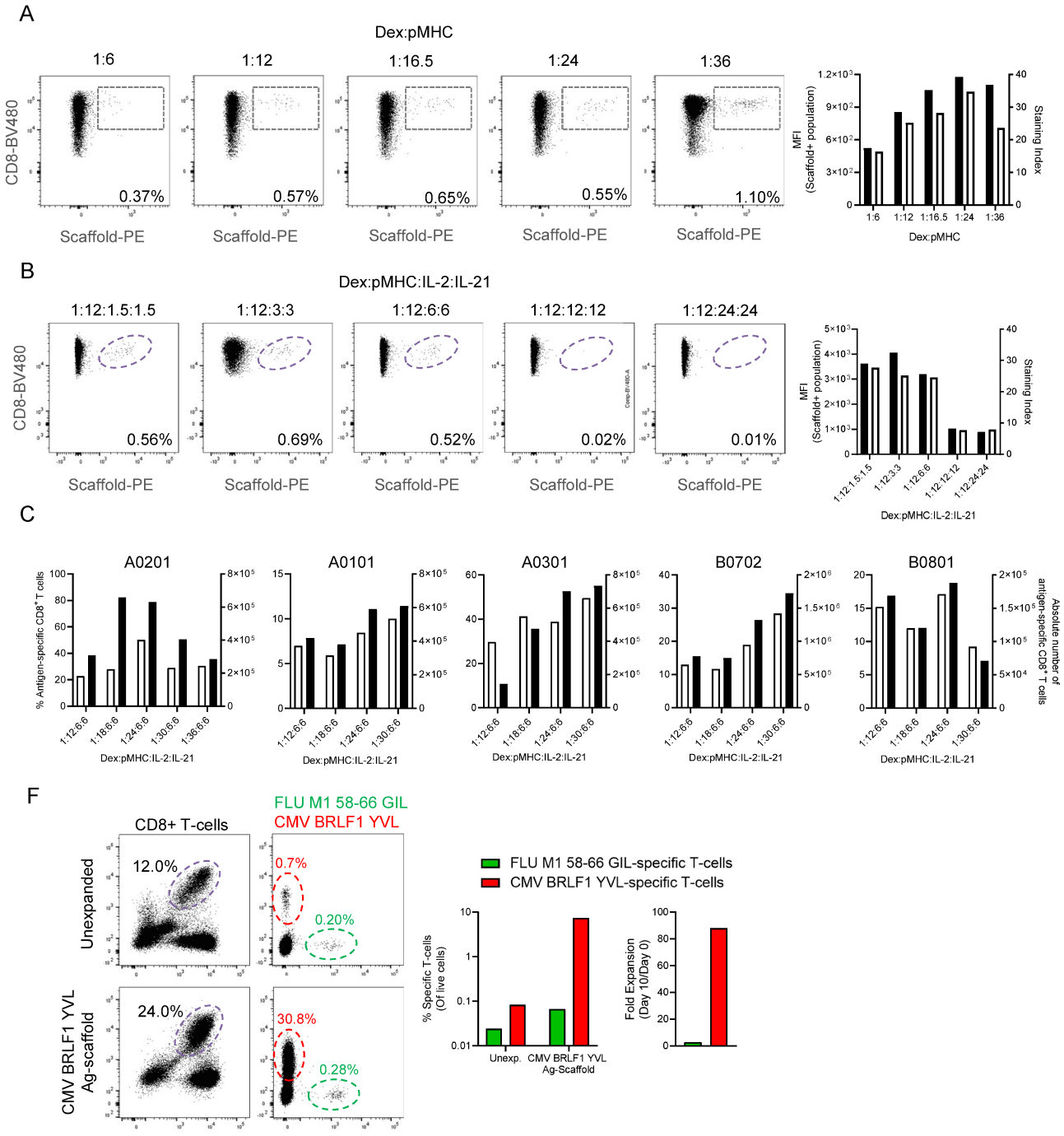

Suppl. Figure S1 | Ag-scaffolds bind to specific T-cells via attached pMHC I and delivers co-attached co-stimulation and cytokines

(A) Binding of PE-labeled dextran-backbone, with varying amounts of pMHCs, to HLA-A0101 CMV pp65 VTE-specific T-cells (~0.5%). Ratios were compared in median fluorescent intensity (MFI) and staining index (SI). CD8 T-cells were labeled with BV480. **(B)** T-cell binding of a 1:12 dextran:pMHC in combination with varying amounts of IL-2:IL-21 was compared based on MFI and SI **(C)** Frequency (left Y-axis) and number (right Y-axis) of HLA-A0201 CMV pp65 NLV-, HLA-A0101 CMV pp50 VTE-, HLA-A0301 FLU NP ILR-, HLA-B0702 CMV pp65 TPR-, HLA-B0801 EBV RAK-specific T-cells post-expansion with an unlabeled dextran backbone with varying amounts of pMHC and 6:6 IL-2:IL-21 (dextran:pMHC:IL-2:IL-21). **(F)** Frequency of CD8+, HLA-A0201 CMV BRLF1 YVL- (red) and FLU M1 58-66 GIL-specific T-cells (green) before and after expansion of healthy donor PBMCs with a CMV BRLF1 YVL Ag-scaffold. Expansion of FLU M1 58-66- (green) and CMV BRLF1 YVL-specific T-cells (red) was compared in % specific T-cells of total live cells and fold expansion (Day 10/Day 0).

Supplementary Figure S2

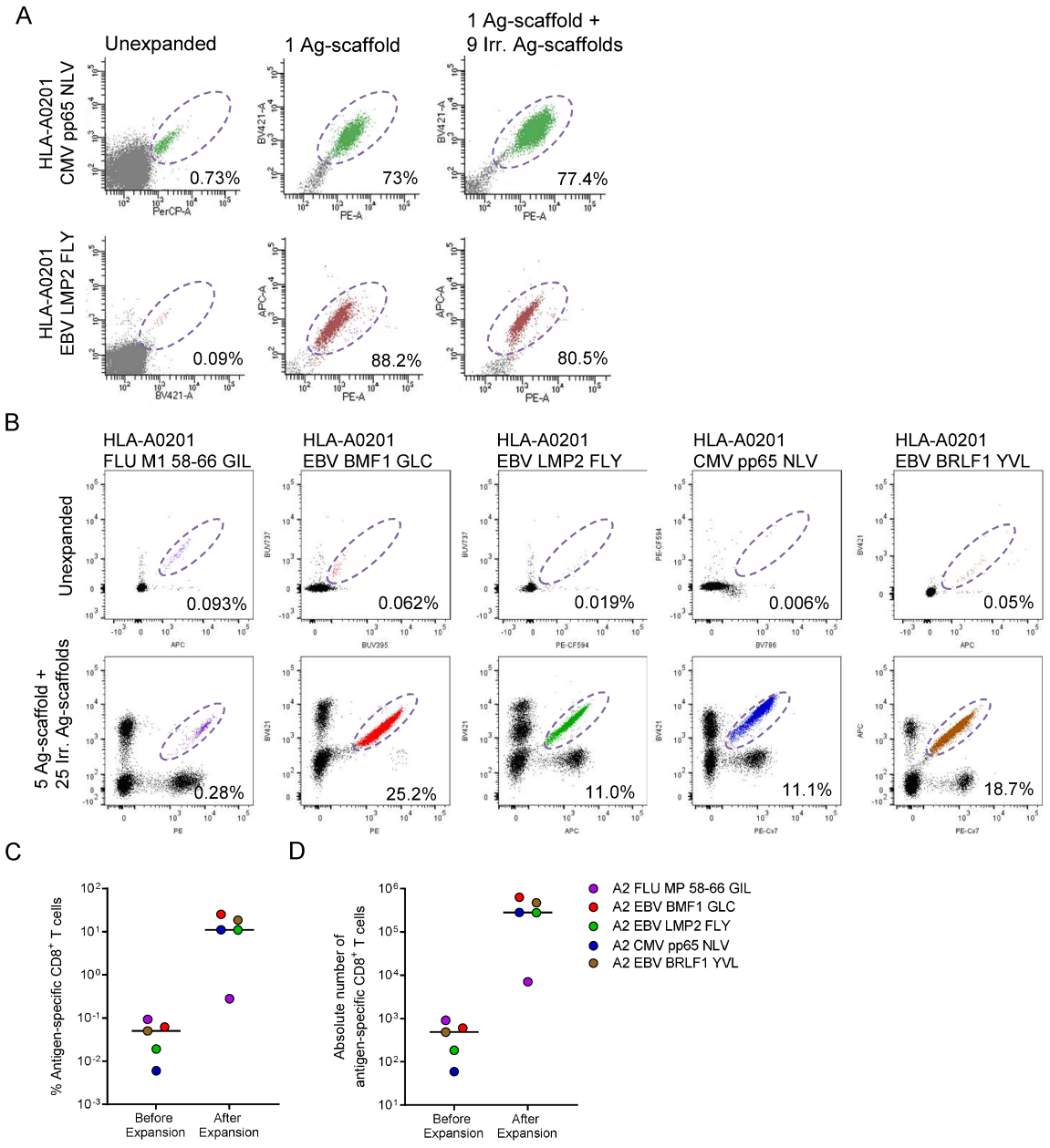

Supplementary Figure S2 | Ag-scaffolds can expand multiple specificities simultaneously in one culture

(A) HLA-A0201 CMV pp65 NLV- (~0.73, green) and EBV LMP2 FLY-specific T cell populations (~0.09%, red) from one healthy donor were expanded in parallel using either a single relevant Ag-scaffold or a combination of one specific Ag-scaffold and nine Ag-scaffolds with irrelevant pMHC in 1/10 of the standard Ag-scaffold concentration. Specific T cells were marked with tetramer staining with varying color-combinations. **(B)** HLA-A0201 FLU MP 58-66 GIL- (~0.09%, purple), EBV BMF1 GLC- (~0,06%, red), LMP2 FLY- (0.02%, green), CMV pp65 NLV- (~0.006%, blue), or EBV BRLF1 YVL-specific T cells (~0.05%, brown) from one healthy donor were expanded simultaneously in a single culture using five relevant Ag-scaffolds and 25 Ag-scaffolds with irrelevant pMHC in 1/10 of the standard Ag-scaffold concentration. Specific T cells were marked with tetramer staining using combinatorial encoding. **(C)** Frequency and **(D)** absolute number of antigen-specific CD8+ T cells before and after Ag-scaffold expansion. The data is representative of three independent experiments.

Supplementary Figure S3

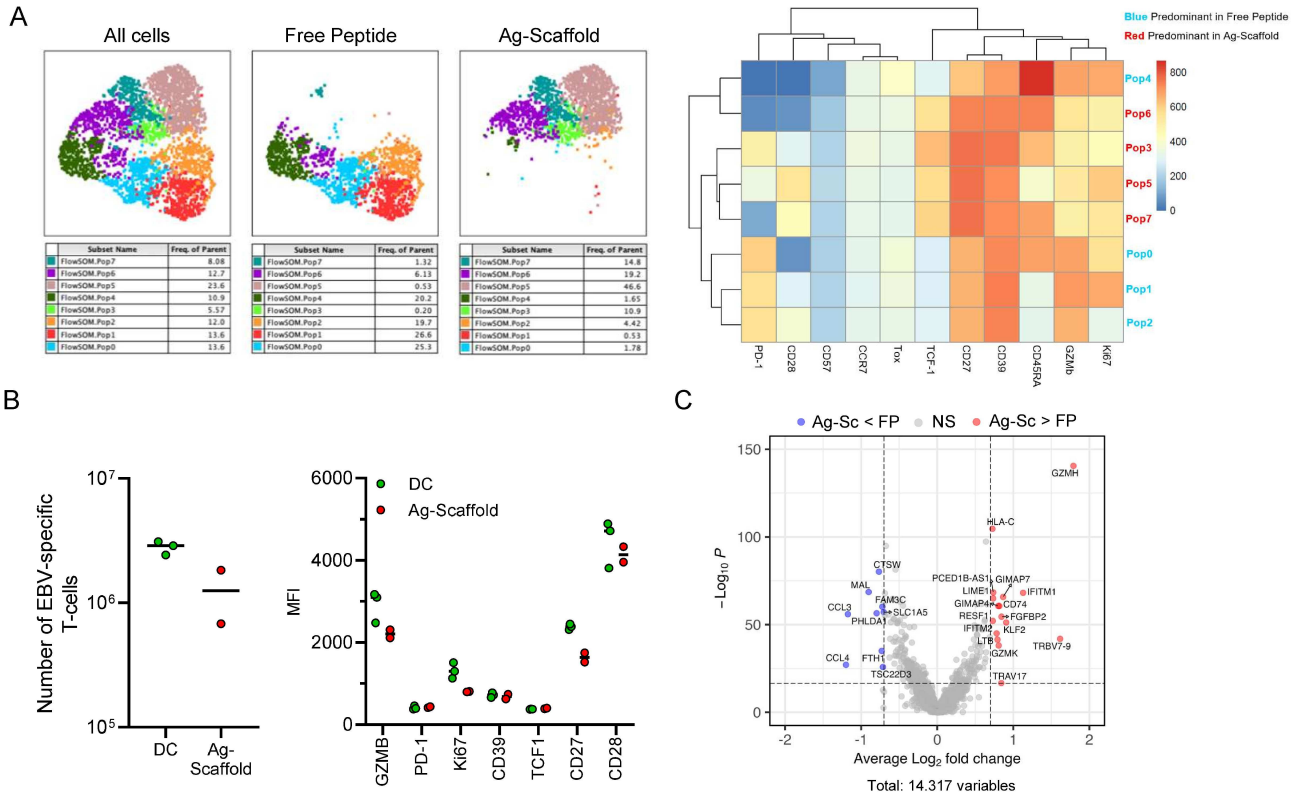

Supplementary Figure S3

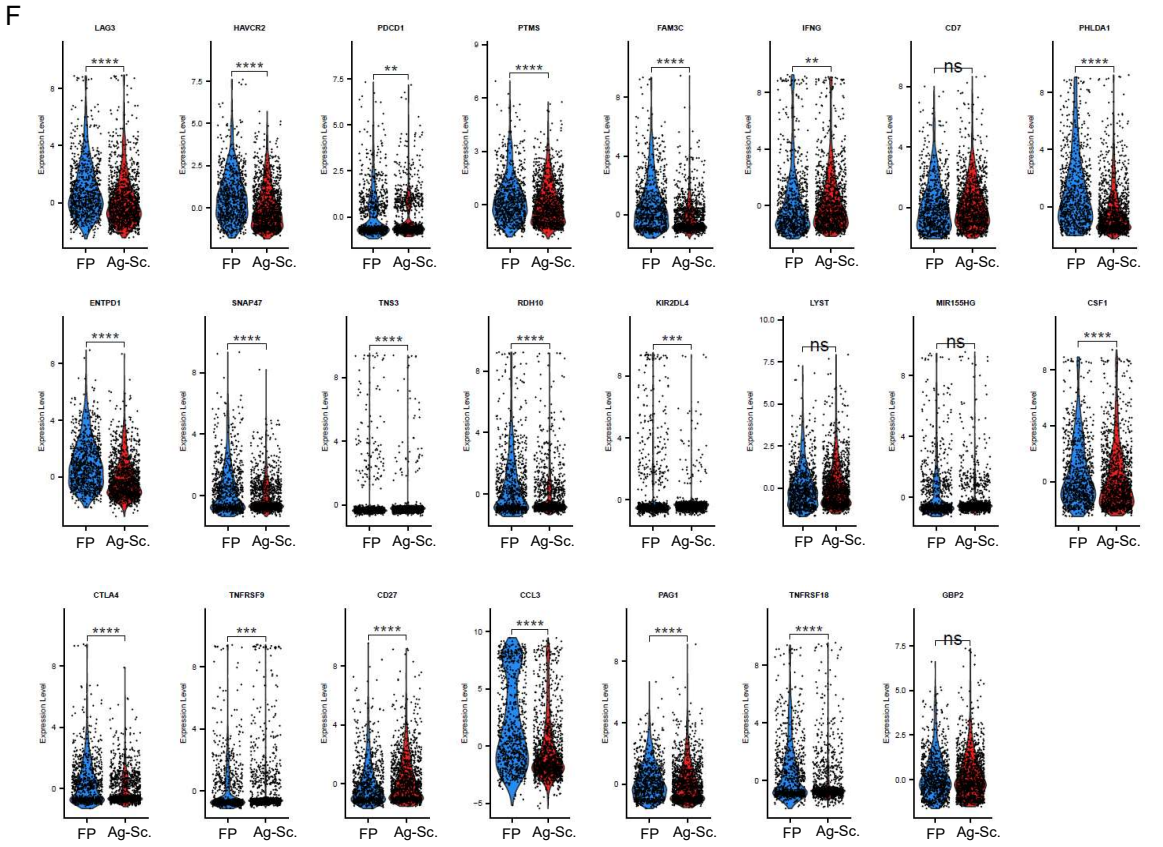

Supplementary Figure S3 | Extended phenotypic, transcriptional and TCR clonal distribution analysis of Ag-scaffold and free peptide-expanded T-cells

(A) FlowSOM unsupervised clustering analyses of HLA-A0101 CMV p50 VTE-specific T-cells expanded in duplicate from two healthy donors with either Ag-scaffold or free peptide. Specific T-cells were identified by tetramer-staining and these were characterized using an antibody panel covering various $CD8^+$ T-cell differentiation states **(B)** Number HLA-A0201 EBV BMLF1-specific T-cells following 10-day expansion with either dextran:pMHC:IL-2:IL-21 Ag-scaffold (n = 2) or peptide-pulsed autologous moDCs (n = 3) from healthy donor PBMCs and a phenotypic comparison of the resulting T-cell products (MFI) **(C))** Single-cell transcriptomic and analysis of unexpanded or Free Peptide- and Ag-Scaffold-expanded HLA-A0301 Flu NP IRL-specific and HLA-B0702 CMV pp65 TPR-specific T cells from two healthy donor BCs, respectively **(D)** Single-cell transcriptomic and **(E)** phenotypic analysis of unexpanded, free peptide-based or Ag-Scaffold-expanded HLA-A0301 Flu NP IRL-specific and HLA-B0702 CMV pp65 TPR-specific T cells from two healthy donors. **(F)** Expression of each individual gene (n = 23) that were included in calculation of the dysfunctional score in Free peptide- (FP) and Ag-scaffold (Ag-Sc)-expanded HLA-A0301 Flu NP IRL-specific and HLA-B0702 CMV pp65 TPR-specific T cells from two healthy donors. Mean expressions were compared in an unpaired, non-parametric Mann-Whitney test and $p > 0.05$, $p < 0.01$, $p < 0.001$ and $p < 0.0001$ is indicated as ns, **, *** and ****, respectively. **(G)** TCR clonal distribution in the antigen-specific T cell population in unexpanded, Free peptide-based or Ag-Scaffold-expanded PBMCs from two healthy donors. Circle size corresponds to clonal frequency out of all clones detected.

Supplementary Figure S4

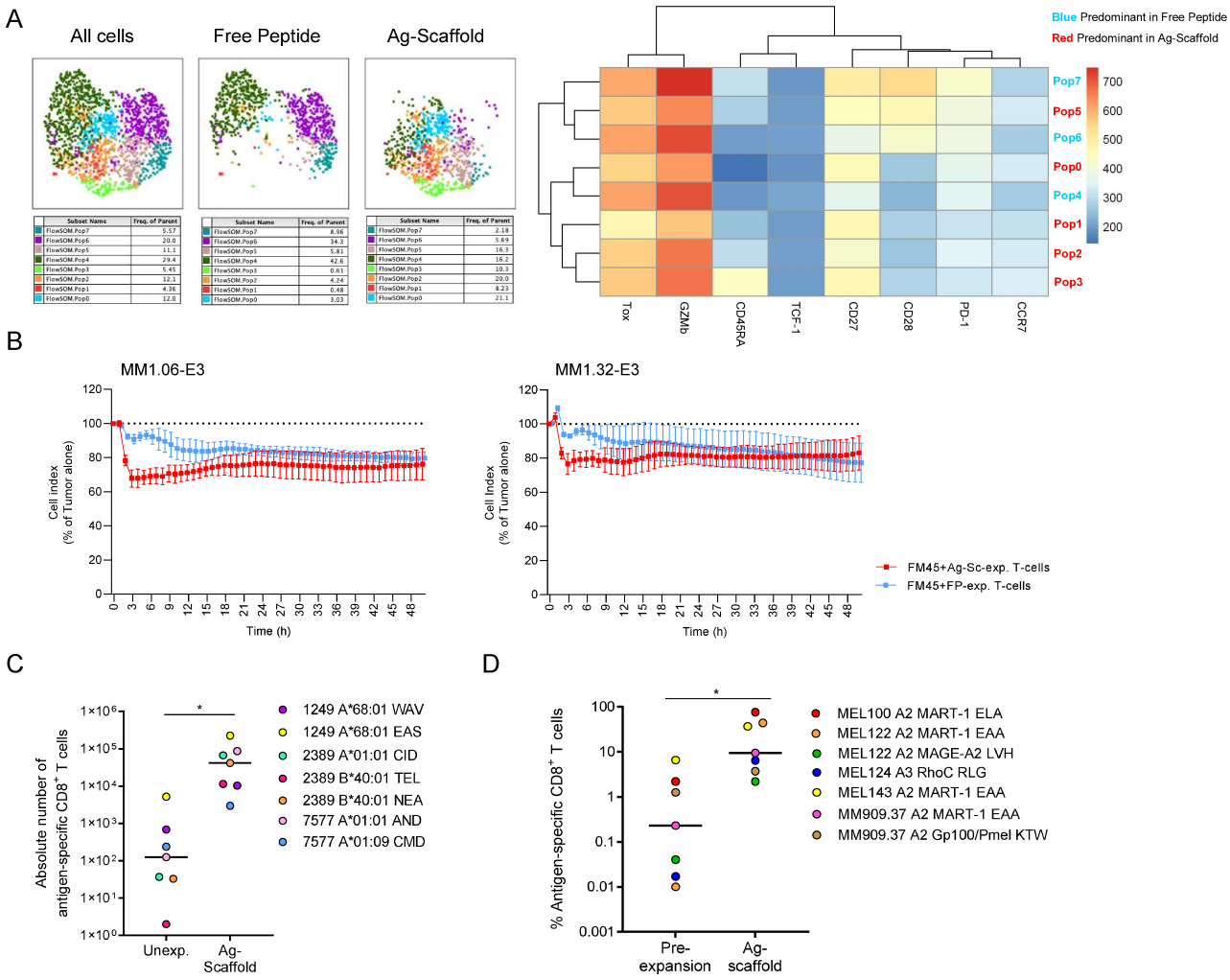

Supplementary Figure S4 | Phenotypic and functional analysis of Ag-scaffold- and free peptide-expanded tumor-specific T-cells

(A) Identification of seven distinct populations among A0101 CMV p50 VTE-specific T-cells expanded in duplicate from two healthy donors with either Ag-scaffold or free peptide, using FlowSOM unsupervised clustering analyses. Specific T-cells were identified by tetramer-staining and these were characterized using an antibody panel covering various $CD8^+$ T-cell differentiation states **(B)** Survival of HLA-A0201-negative FM45 melanoma tumor cells (Cell Index as a relative measure of impedance presented as % of tumor alone) when co-cultured with Ag-scaffold (red) or free peptide-expanded (blue) tumor-specific T-cells from MM1.06- and 32-E3 in a 4:1 E:T ratio. **(C)** Number of neoantigen-specific T-cells before (Unexp.) and after Ag-scaffold-based expansion from PBMCs from three bladder cancer patients **(D)** Frequency of shared melanoma-antigen-specific T-cells in tumor digest/fragment from five metastiatic melanoma patients, pre-expanded with αCD3/CD28 beads (Pre-expansion) only or Ag-scaffold-expanded following pre-expansion.

Supplementary Figure S5

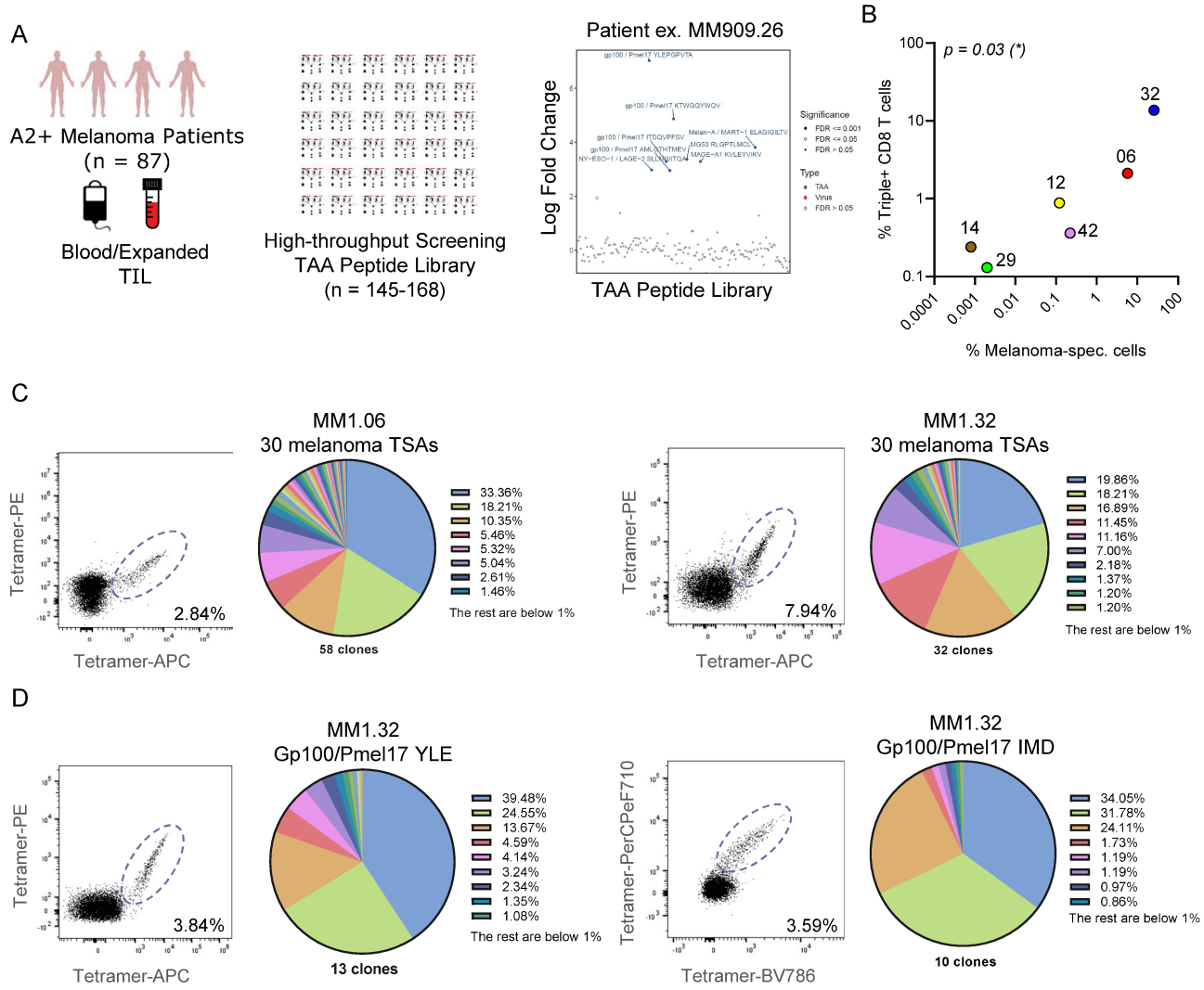

Supplementary Figure S5 | Identification of TSA-specific T-cells in melanoma patients and TCR clonal distribution in Ag-scaffold-expanded TSA-specific T-cells

(A) TILs and PBMCs from a combined cohort of 87 HLA-A0201-positive patients with metastatic melanoma were screened for T-cell reactivity against a library of 145-168 HLA-A0201-restricted shared melanoma antigens using either combinatorial encoded or barcode-labeled pMHC multimers. **(B)** Correlation between the frequency of TNFαIFNyCD107a Triple+ and TSA-specific T-cells, p-value according to a Spearman's rank test. **(C)** TCR clonal distribution in Ag-scaffold-expanded MM1.06 (left) and MM1.32 (right) TSA-specific T-cells. In MM1.06 and -32, the top 8 and 10 clones contribute to 81.8 and 90.5% of the antigen-specific T-cell population, respectively. **(D)** TCR clonal distribution in Ag-scaffold-expanded MM1.32 HLA-A0201 Gp100/Pmel17 YLE- (left) and IMD-specific (IMD) T-cells.

Supplementary Figure S6

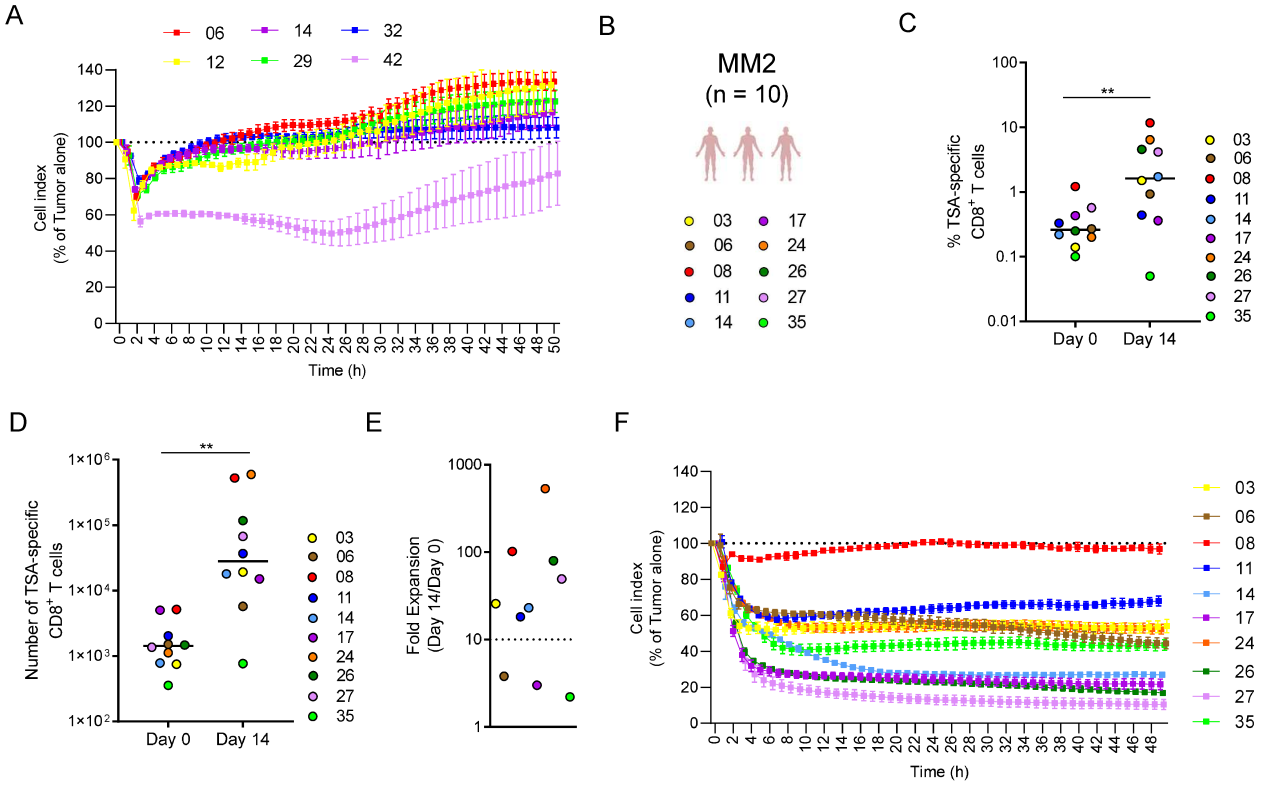

Supplementary Figure S6 | Additional expansion of tumor-specific T-cells from patient PBMCs using the multi-targeting shared melanoma Ag-scaffold

(A) Survival of A0201-negative FM45 melanoma tumor cells (Cell Index as a relative measure of impedance presented as % of tumor alone) when co-cultured with Ag-scaffold-expanded T-cells from the six melanoma patients (MM1) in a 4:1 effector:target ratio. **(B)** PBMCs from a cohort of ten patients with metastatic melanoma (MM2) were expanded with the multi-targeting shared melanoma Ag-scaffold, comprising 30 Ag-scaffolds carrying the 30 selected TSAs on HLA-A0201. **(C)** Frequency and **(D)** number of melanoma-specific T-cells pre- (Day 0) and post-expansion (Day 14). **(E)** Fold expansion (FE = Day 14/Day0). **(F)** Survival of HLA-A0201-positive FM93/2 melanoma tumor cells when co-cultured with Ag-scaffold-expanded T-cells from ten melanoma patients (MM2) in E:T ratio 1:4.

Supplementary Table 1

	ESTDAB/ECACC ID	HLA Type (A, B, C)	TSA-expression
FM45	ESTDAB-011 ECACC13012410	A6801, A2401 B5301, B5701 C0602, C0401	https://www.culturecollections.org.uk/media/78959/13012410_fm-45_characterisation-data.pdf
FM3	ESTDAB-007 ECACC13012407	A0201 B0702, B4402 C0501	https://www.culturecollections.org.uk/media/77636/13012407_fm-3_characterisation-data.pdf
FM93/2	ESTDAB-033 ECACC13012419	A0201 B4001, B4402 C0304, B0501	https://www.culturecollections.org.uk/media/78182/13012419_fm-93-2_characterisation-data.pdf

Supplementary Table 2

Antibody and SA-conjugate list

Tetramer staining:

CD3-FITC, SK7, BD 345764

CD8-BV480, RPA-T8, BD 566121

CD8-PECy5, RPA-T8, BD 561951

PE-SA, Biolegend 405204

APC-SA, Biolegend 405243

BV421-SA, BD 563259

PE-CF594-SA, BD 562284

PECy7-SA, Biolegend 405206

BV650-SA, BD 563855

BUV737-SA, BD 564293

BV786-SA, BD 563858

PerCPeF710-SA, eBioscience 46-4317-82

BUV395-SA, BD 564176

BV711-SA, BD 563262

Dump channel staining:

CD4-FITC, BD 345768

CD14-FITC, BD 345784

CD19-FITC, BD 345776

CD40-FITC, Serotech MCA1590F

CD16-FITC, BD 335035

Phenotype staining:

CD3-BV786, SK7, BD 0349301

CD8-BV480, RPA-T8, BD 566121

TOX-APC, REA473, Miltenyi Biotec 5201005445

PD-1-BV421, EH12.1, BD 565024

GZMb-AF700, QA16A02, Biolegend B304753

CD28-BUV737, CD28.2, BD 612815

CD27-BV605, O323, Biolegend B338033

TCF-1-PE, S33.966, BD 564217

ɔkine staining:

CD107a-PE, H4A3, BD 555801

TNFα-PECy7, MAb11, Biolegend 502930

IFNγ-APC, 25723.11, BD 341117

Supplementary Table 3

Figure 2A	ICOS	OX40L	CD5	IL-1	IL-6	IL-10	IL-15	IL-21	IL-7	IL-12p70	CD47
OX40L	43,8										
CD5	26,2	24,7									
IL-1	**67,2**	35,6	22,6								
IL-6	11,4	0,43	6,32	33							
IL-10	26,2	26,6	4,89	35,7	26,7						
IL-15	24,1	15,6	10,9	2,48	4,36	22,5					
IL-21	**61,9**	17,5	6,4	34,2	28,5	19,6	7,36				
IL-7	23,2	33,9	7,99	10,9	7,06	21,8	0,95	12,4			
IL-12p70	13,9	34,3	13	**59,8**	38,9	23,4	14	2,24	8,68		
CD47	20,5	35,4	25,2	41,7	37,3	0,48	6,49	7,23	3,21	50,6	
IL-2	**77,4**	41,8	22	51,1	23,8	53,8	26,5	**82,3**	10,7	9,91	30

Figure 2B	ICOS	OX40L	CD5	IL-1	IL-6	IL-10	IL-15	IL-21	IL-7	IL-12p70	CD47
OX40L	22,6										
CD5	9,93	6,04									
IL-1	**31,4**	12,4	4,18								
IL-6	3,79	0,056	5,38	31,3							
IL-10	12,5	14,9	1,35	26,9	13,6						
IL-15	9,29	5,82	1,02	0,49	1,23	8,87					
IL-21	**41,2**	6,8	0,65	14,4	14,4	7,01	1,98				
IL-7	3,36	11,1	1,83	2,57	1,05	6,03	0,22	2,68			
IL-12p70	9,14	2,32	4,54	**16**	14,2	12	4,87	12,5	0,85		
CD47	9,63	26,7	4,97	11,4	18,8	0,24	1,62	3,23	0,98	9,79	
IL-2	**38,2**	19	3,95	16,4	8,92	19,4	7,38	**30,9**	0,69	2,97	5,71

Figure 2C	ICOS: IL-2	ICOS: IL-21	ICOS: IL-1	IL-2: IL-21	IL-1: IL-12p70
Ag-scaffold -B7	88,4	27	69,1	**96**	34,6
Ag-scaffold +B7	79,2	52	51,5	77,6	49,2

Figure 2D	ICOS: IL-2	ICOS: IL-21	ICOS: IL-1	IL-2: IL-21	IL-1: IL-12p70
Ag-scaffold -B7	15,7	7,49	5,84	**25,8**	10,6
Ag-scaffold +B7	4,4	16,3	13,9	20,1	22,3